3D Numerical Analysis for Impedance Calculation and High Performance Consideration of Linear Induction Motor for Rail-guided Transportation

CUONG Ninh Van[1]*, Yuta Yamamoto[1] and Takafumi Koseki[1]

[1]Department of Electrical Engineering, School of Engineering, The University of Tokyo, Japan
*Corresponding author, E-mail: ninh.cuong@koseki.t.u-tokyo.ac.jp

Abstract

In this paper, the authors describe the method of calculating the impedance of Linear Induction Motor (LIM) for rail-guided transportation using magnetic vector potential that can be obtained from three-dimensional numerical analysis. Based on this method, high performance and power saving for some models of current research trends in LIM concerning the mechanical clearance and secondary reaction plate construction are discussed.

1. Introduction

In the past few years, the construction of new urban subway lines using Linear Induction Motor (LIM) has been developed, especially in Japan and Korea. Significant advantages of LIM are: direct thrust without gears and links, simple structure, and easy maintenance. In addition, LIM reduces the sectional area of tunnel and the large grad-ability enables the minimum length of the route. However, different from rotating motor, LIM has special characteristics and inherent problems because of the non-continuity of the magnetic field. Longitudinal end effect and transverse edge effect are two major electromagnetic phenomena of LIM, which makes the analysis, design and control of this motor difficult. While longitudinal end effect is strongly affected by slip frequency and the length of mechanical clearance, transverse edge effect is strongly affected by the construction of secondary reaction plate. Thus, in the transportation system using LIM, mechanical clearance and secondary reaction plate are important design factors due to their influence on not only the operation cost but also the construction cost.

In LIM, the experiments for analysis and design are difficult to carry out due to the requirement of construction features. The analysis research of longitudinal end effect and transverse edge effect in LIM is generally based on an idealized mathematical model that has some restrictions [1]-[3]. The first restriction is that the longitudinal end effect is caused by finite length of primary that requires LIM the full modeling in analysis. The second restriction is two-dimensional (2-D) analysis cannot express the influence of transverse edge effect which is caused by the finite widths of the primary and secondary part. Hence, in order to evaluate the characteristics of LIM, the three-dimensional (3-D) analysis with full-length model is necessary.

In this paper, 3-D numerical analysis with full model of LIM is used to consider the generated forces and efficiency of this motor owing to the mechanical clearance and the construction of secondary reaction plate. Firstly, the authors describe the method for motor's impedance calculation from vector potential which can be obtained from numerical analysis. Secondly, by applying this method, characteristics of LIM, including generated force and power generation, with different models concerning the influence of mechanical clearance and secondary reaction plate will be discussed. Finally, improving efficiency and power factor of LIM will be clarified.

2. 3-D LIM model and analysis conditions

In order to consider the characteristics of this motor, LIM model is described in Fig.1, which includes front view of full model, lateral view and construction of the one-phased coil in 3-D. In addition, other parameters and analysis conditions are summarized in Table 1. It must also be noted that the end winding with complex shape must be taken into account. Therefore, the characteristics of LIM in this model are quite similar to the actual LIM. However, because of the requirement of transient analysis of the 3-D full modeling, sufficient computer memory and solving are necessary.

The total pole of this model is 8 while the pole pitch length is 280.8 mm, so the synchronous speed is about 11.8 m/s (42.3 km/h). As shown in Table 1, the analysis is taken in a constant slip frequency of 2.1 Hz, so the primary core is moving on secondary part with constant speed of 10.6 m/s (38.2 km/h). Furthermore, in this model, three-phased sinusoidal current at constant frequency is applied to the coils of LIM and each phase coil is connected to the others in series.

In our experiments, the simulations were conducted with ELF/MAGIC software in three-dimensional electromagnetic field analysis and the integral element method has been used [4]-[5]. In each model of simulation, the computation has been carried out in eight periods of the current wave-form; the electrical angle step width at each time step is 10 degree. This means 288 steps were calculated (36 steps × 8 periods = 288 steps).

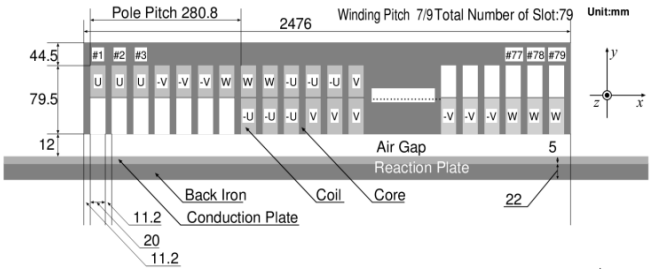

(a) Front view of the full model

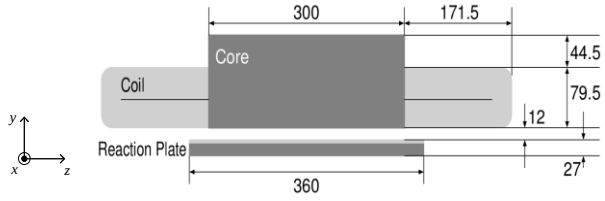

(c) Lateral view

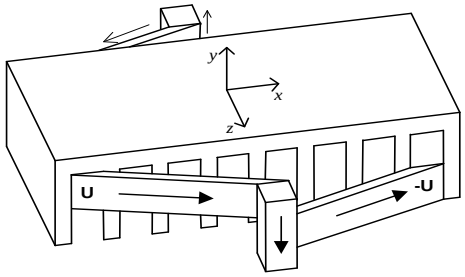

(c) Three dimensions of one U-phase coil model (Extracted process from full model)

Fig. 1. Model of LIM for rail-guided transportation

Table 1. The analysis conditions for LIM

Symbols	Items	
f_n	Normal frequency [Hz]	21.0
f_s	Slip frequency [Hz]	2.1
f_{ns}	Rated slip frequency [Hz]	3.0
v_s	Normal speed [km/h]	38.2
i_1	Primary source current [A]	170
	Material of conduction plate	Cu
μ_r	Relative permeability in primary/back iron	1000
σ	Conductivity in primary/back iron	0.0

3. LIM impedance calculation method

In LIM, impedance calculation is a hard topic because the influence of equivalent circuit parameters of LIM strongly depends on the operational speed, especially at high-speed operation. Most of the other researchers have found out that the impedance of LIM is based on the model of rotary induction motor with longitudinal end effect and transverse edge effect coefficients which can be counted for as the function of operational speed, goodness factor and secondary structure parameter [3]. Although this method can demonstrate the influence of the mutual inductance and secondary resistance to the longitudinal end effect and transverse edge effect, it must be taken out at some approximate regulations. Defining the impedance value from vector potential is difficult because of the number of calculations; however, we can obtain the high accurate values by adjusting the number of meshes in numerical analysis. The details of this calculation method can be seen in Fig. 2. Firstly, with the LIM model described in section 2, magnetic vector potential A will be obtained from the electromagnetic field analysis. After that, electric scalar potential φ is calculated from A by Maxwell equations. Then, the back electromagnetic force (EMF) of each coil side and the impedance, including absolute value and power factor will be determined accordingly. As the analysis condition mentioned in section 2, it should be noted that high resolution for the voltage and current phase can be obtained thanks to the analysis conducted every 10 electrical angle.

In general, the impedance of the number *i-th* coil is consisted of self-inductance $X_{ii}(i=j)$, mutual inductance $X_{ij}(i \neq j)$, and coil wingding resistance R_i and which can be described as the following equation

$$Z = \begin{bmatrix} R_1 & 0 & \cdots & 0 \\ 0 & R_2 & \cdots & 0 \\ \vdots & \vdots & \vdots & \vdots \\ 0 & 0 & 0 & R_n \end{bmatrix} + j\omega \begin{bmatrix} X_{11} & X_{12} & \cdots & X_{1n} \\ X_{21} & X_{22} & \cdots & X_{2n} \\ \vdots & \vdots & \vdots & \vdots \\ X_{n1} & X_{n2} & \cdots & X_{nn} \end{bmatrix} = \begin{bmatrix} Z_{11} & Z_{12} & \cdots & Z_{1n} \\ Z_{21} & Z_{22} & \cdots & Z_{2n} \\ \vdots & \vdots & \vdots & \vdots \\ Z_{n1} & Z_{n2} & \cdots & Z_{nn} \end{bmatrix} \quad (1)$$

Current and voltage applied to the coil number #*n* are $I = [I_n]$ and $V = [V_n]$, so the impedance matrix can be obtained as following

$$\begin{bmatrix} V_1 \\ V_2 \\ \vdots \\ V_n \end{bmatrix} = \begin{bmatrix} Z_{11} & Z_{12} & \cdots & Z_{1n} \\ Z_{21} & Z_{22} & \cdots & Z_{2n} \\ \vdots & \vdots & \vdots & \vdots \\ Z_{n1} & Z_{n2} & \cdots & Z_{nn} \end{bmatrix} \begin{bmatrix} I_1 \\ I_2 \\ \vdots \\ I_n \end{bmatrix} \quad (2)$$

or

$$V = ZI \quad (3)$$

Fig. 3 shows that in numerical analysis with a current source, the induced primary terminal voltages in each coil can be determined by direct integration over the coil side of the distribution of the magnetic vector potential through Maxwell equation as shown in Eq. (4) and (5)

$$\mathbf{B} = \nabla \times \mathbf{A} \quad (4)$$

$$\nabla \times \mathbf{E} = -\frac{\partial \mathbf{B}}{\partial t} \quad (5)$$

where **B**, **A**, **E** represent for magnetic flux density, magnetic vector potential and electric field.

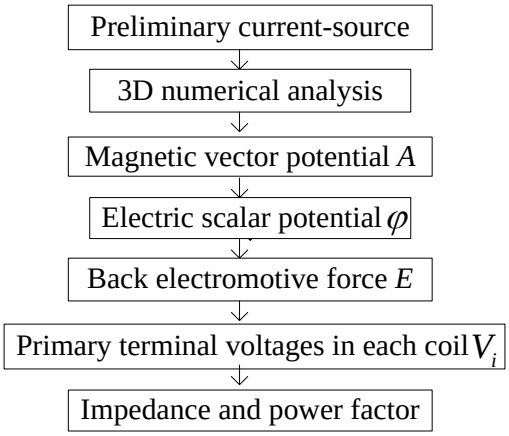

Fig. 2. Flowchart of impedance calculation

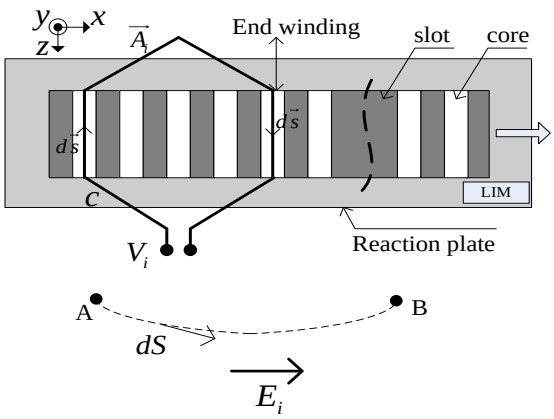

Fig. 3. Assumption of integral route in line integral of magnetic vector potential

Thus, the electric field is obtained from magnetic vector potential as follows:

$$\nabla \times \mathbf{E} = -\frac{\partial}{\partial t}(\nabla \times \mathbf{A}) \tag{6}$$

In addition, the relation between the terminal voltage in each coil and the electric field is expressed below:

$$V_i = \int_c \vec{E_i}.d\vec{S} \tag{7}$$

So from (6) and (7) we can obtain terminal voltage as follows:

$$V_i = -j\omega \int_c \vec{A_i}.d\vec{S} \tag{8}$$

From the V_i above, the absolute value of the impedance of the equivalent circuit is calculated as:

$$|Z_i| = \frac{|V_i|}{|I_i|} \tag{9}$$

and the power factor *p.f.* is calculated by using the phase difference between the input current and the back EMF:

$$p.f. = \cos\Delta\theta \tag{10}$$

With the different operating point of LIM, using the above process, the impedance can be determined as the function of the secondary speed, and these results are significant when considering the power saving in LIM operation.

4. Analysis results and discussion

In this part, the authors describe the characteristics of target LIM at the operating point near rated slip frequency. The models of LIM are based on the requirement of reduction of longitudinal end effect and transverse edge effect to obtain high efficiency and power factor. For the purpose of comparison, three models have been used, Fig. 4.

- Standard model (**A**): is the model based on the recently used model of LIM for Linear Metro system in Japan (also described in section 2)
- Short-gap model (**B**): is the model with the same parameter as model **A** but with reduction of mechanical clearance
- Full-cap model (**C**): is the model with full cap for secondary reaction plate and short-gap with the demand of reduction of transverse edge effect and increase thrust and efficiency [7].

By using the impedance calculation method described in section 3 of this paper, the performance of three models has been evaluated through the comparison of generated force and power generation.

Fig. 5 shows the characteristics of two-dimensional forces of LIM including longitudinal and normal forces variations in time steps. With the initial current input, in order to suppress the rapid decrease of magnetic flux interlink between primary and secondary part, eddy current in the secondary side becomes larger. This process makes the transient process bigger and the 2-D force at steady state smaller in comparison with the value of transient process. In this model, it is found that we need 150 - 200 step calculations in order to obtain thrust at the steady state.

Fig. 6 demonstrates one cycle of electrical angle scalar potential φ (corresponding to the flux linkage of the coil), which is obtained by vector potential *A* along coil line and the applied current at the steady state. Assume that each phase of scalar potential in Fig. 6 is sine wave; its effective value is used to calculate the induced single phase terminal voltage $V_i(i = u, v, w)$.

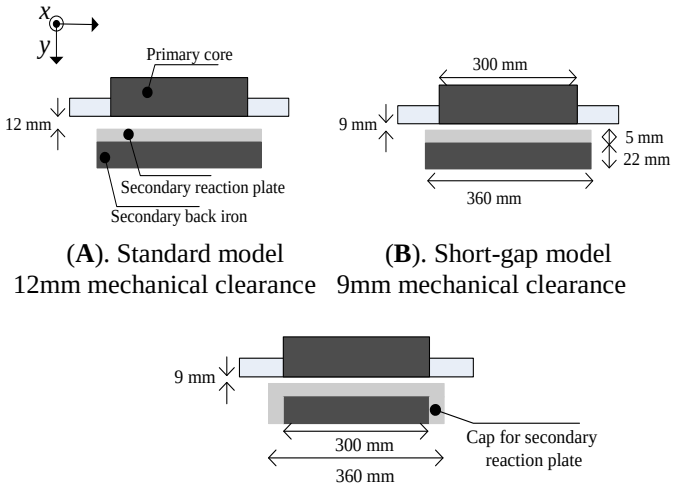

(**A**). Standard model 12mm mechanical clearance

(**B**). Short-gap model 9mm mechanical clearance

(**C**). Full-cap model 9mm mechanical clearance and full-cap

Fig. 4. Analysis model for high performance

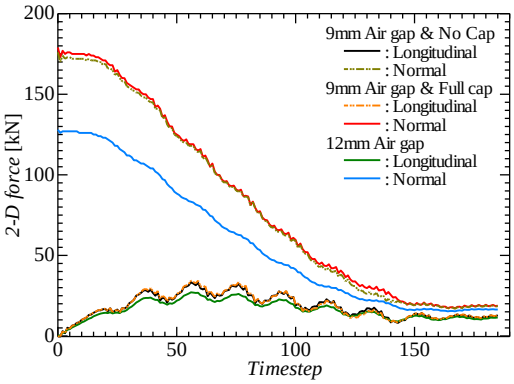

Fig. 5. 2-D force characteristics of 3 models of LIM at motor starting transient

Furthermore, as shown in equation (9) and (10), from the ratio of absolute value of V_i to input current I_i we can calculate the absolute value of impedance, and also from phase difference between V_i and I_i we can determine the power factor of this motor.

Considering longitudinal end effect and transverse edge effect, from 3-D numerical analysis, not only the impedance value but also other characteristics of three models are obtained as shown in Table 2. In this simulation, because of conductivity in iron core setting at 0, eddy current loss in iron core can be ignored. So the Joule heat losses in Table 2 replace the eddy current losses in secondary conductor (secondary loss) and primary copper losses. While power factor are determined as (10), the efficiency can be calculated as following:

$$\eta = \frac{F_x v_2}{F_x v_2 + P_{loss}} \tag{11}$$

Because of the ignorance of the eddy current loss at the iron core, it should be noted that the efficiency in (11) is a little higher than the LIM in actual operation.

From the result in Table 2 we can see that, as the mechanical clearance reduces, from model **A** to model **B**, the reluctance and leakage flux of the magnetic circuit decrease and magnetizing inductance increases. Consequently, much less excitation current is required. Even under the same input current, the more efficient transfer of magnetic energy between the primary and secondary side makes thrust and normal force increase. The increase of inductance not only makes power factor decrease, but with the decrease of excitation current it also leads to the reduction of secondary power loss, which results in increase of the efficiency. The results show that, at the mechanical clearance 12 mm in model **A** and 9 mm in model **B**, the power losses decrease by 14% from 38 kW to 32.7 kW, and the efficiency increases by 2% from 75.7% to 79.7%. With the reduction of mechanical clearance, slip in optimal design must also be reduced. However, in our simulation, slip is set up at the same value 0.1, so it makes the value $\eta * p.f$ in model **A** bigger than in model **B**.

As the expression in Maxwell stress tensor, normal force is proportional to the square of the *y*-component of magnetic flux density at the air gap B_y. Furthermore, under certain gap cross-section, magnetic flux density B_y is inversely proportional to the gap between the cores g [8]. Therefore, if the mechanical clearance is reduced from 12mm to 9mm, the gap between the cores is reduced from 17mm to 14mm and normal force increases nearly 50%, as shown in Eq.12 and Eq.13. However, different from this theory, due to the shielding effect of eddy current in conduction plate, the result from 3-D analysis shows that normal force increases of 10% from 17.1kN to 18.1kN.

$$F_y \propto B_y^2 - \frac{1}{2}\left|\vec{B}\right|^2 \propto B_y^2 (\because B_y^2 \gg B_x^2, B_z^2) \tag{12}$$

$$\frac{F_{y(\mathbf{B})}}{F_{y(\mathbf{A})}} \propto \left|\frac{B_{y(\mathbf{B})}}{B_{y(\mathbf{A})}}\right|^2 \propto \left|\frac{g_{\mathbf{A}}}{g_{\mathbf{B}}}\right|^2 = \left(\frac{17}{14}\right)^2 \simeq 1.47 \tag{13}$$

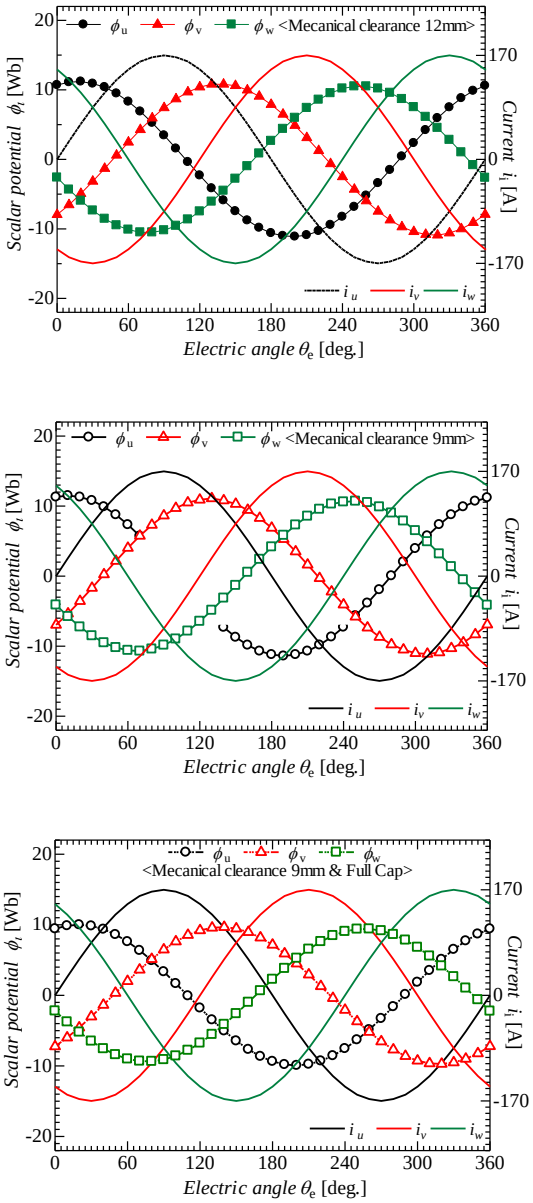

Fig. 6. Absolute value and phase relation between scalar potential and applied current in steady state in 3 models

Table 2. Characteristics of different models of LIM by 3-D numerical analysis

Model	A	B	C
Thrust [kN]	11.2	12.1	12.3
Normal force [kN]	17.1	18.8	19.1
Joule heat [kW]	38.0	32.7	29.7
Power factor	0.47	0.43	0.49
Efficiency [%]	75.7	79.7	81.5
$\eta * p.f.$ [%]	35.6	34.3	39.9

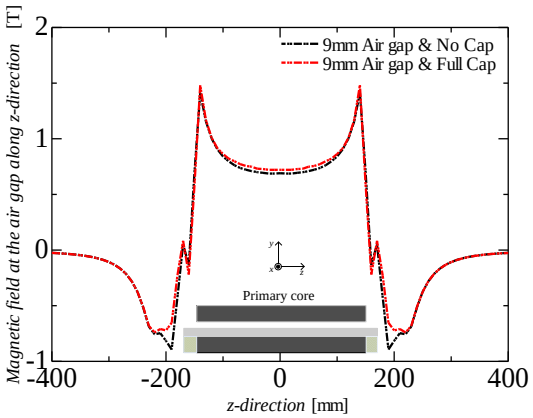

Fig. 7. Distribution of air gap flux density along z-direction

In the design of a LIM having full cap for secondary reaction plate, with the distribution of electric scalar potential and applied current in Fig. 6, we can say that it is a significant method to improve the power factor of LIM. Calculation in Table 2 shows that power factor increases of 14% from 0.43 in model **B** to 0.49 in model **C**. The explanation for this increase can be: when the full cap is used, magnetic flux density at the air gap along *z*-direction is more balanced, the difference of magnetic flux from the center to end of the secondary reaction plate is reduced as shown in Fig. 7. As a result, the secondary current in *z*-direction increases while the influence of *x*-component eddy current decreases. This means that transverse edge effect is reduced due to the using of full cap for secondary reaction plate.

This result shows that using cap for secondary reaction plate is a significant design to get higher thrust and to reduce primary input. However, it must be noted that in order to increase approximately 2% of thrust and efficiency, from model **B** to model **C**, the amount of copper needed had increased of 70%. Therefore, this design is a poor design in term of cost of building. Hence, in order to design an effective motor that can reduce both transverse edge effect and material cost, the designer must consider carefully the advantages and disadvantages of each model.

5. Conclusion

In this paper, the impedance calculation method based on the 3-D numerical electromagnetic analysis is proposed for designing a new LIM for linear subway systems. By using this method, it is possible to determine the characteristics of LIM with high accuracy through a number of tests that cannot be realized under normal conditions.

The 3-D numerical analysis has proved the significant result for obtaining higher thrust and reducing primary input concerning mechanical clearance reduction and using cap for secondary reaction plate. However, reducing mechanical clearance leads to the decrease of power factor, and using cap requires a great more construction cost while the LIM's quality has a little improvement.

Since the construction of mechanical clearance and secondary reaction plate are important design factors from the viewpoint of safety characteristic, cost of building and performance, the method proposed in this paper can be used to find the optimal design of LIM for linear subway system.

In future work, other designs of secondary reaction plate as well as saturation of back iron will be considered by using 3-D numerical analysis and this impedance calculation method.

Acknowledgement

The authors gratefully acknowledge the support of Hitachi, Ltd and Japan Subway Association (JSA) to this work.

References

[1] K. Oberettl, *Three-dimensional theory of linear induction motor considering end-effect and winding distribution*, Arch. f. Elek, vol. 55, April 1973.

[2] A. Lang, *The effect of stray fields on the design and performance of linear induction motors*, PhD. Thesis, Techn. Univ. Braunschweig, Germany, June 1973.

[3] W. Xu, J. G. Zhu, Y. Zhang, Z. Li, Y. Y. Wang, Y. Guo, *Equivalent circuit for single-sided linear induction motor*, IEEE Trans. on industry applications, 2010.

[4] Y. Yamamoto, N. V. Cuong, T. Koseki, *A numerical analysis on variation of forces and impedance of a single-sided linear induction motor to lateral displacement*, Conference of Elec. Eng., Hiroshima, Japan, pp.244-246, March 2012 (In Japanese)

[5] Y. Yamamoto, N. V. Cuong, T. Koseki, *Performance improvement and power-saving of linear induction motors for urban rail-guided transport considering their lateral edge effect*, Conference of Elec. Eng., Tokyo, Japan, December 2012 (In Japanese)

[6] T. Koseki, *Flux synthesizing Linear Induction Motor*, The University of Tokyo, PhD. Thesis, 1991.12. URL: http://repository.dl.itc.utokyo.ac.jp/dspace/handle/2261/1186?mode=full

[7] S. G. Lee, H. W. Lee, S. H. Ham, C. S. Jin, H. J. Park, J. Lee, *Influence of the construction of secondary reaction plate on the transverse edge effect in linear induction motor*, IEEE Trans. Mag., Vol. 45, No. 6, June 2009.

[8] L. Huaiji, Z. Ying, D. Yumei, *Normal force characteristics analysis of single sided linear induction motor*, ICEM 201.